CHAPTER 9 BACK ANALYSIS OF TEST DATA

The experimental results show clearly the advantages of local reinforcement, local prestressing and good packing material. The influence of the packing material has been studied in Chapters 3 and 6. In this chapter, a numerical model of back analysis is described in Section 9.1. Numerical back analysis of the local reinforcement and of the local prestressing are discussed in Sections 9.2 and 9.3 respectively. The numerical back analysis was extended to include the effect of the location of the reinforcement and the effect of the magnitude of the prestress.

9.1 NUMERICAL MODEL OF BACK ANALYSIS

The arrangement of the test apparatus was described in Figure 8.3 in Chapter 8. There were two load plates used in the tests, plate A to apply uniform pressure and plate B for non-uniform pressure. Because the plain concrete pipe performs very well under uniform pressure, the back analysis was only carried out for the tests with the angled load plate B to assess the effect of the reinforcement and of the prestressing at the pipe joint. Although the total applied load was recorded by a load transducer, there was no measurement of the load distribution at the top of the pipe. In the back analysis, a linear load distribution was assumed at each side on the top of the pipe as shown in Figure 9.1 according to the observation from the carbon film paper which was put between the pipe and the load plate during the test. The total applied load on the pipe end was P = 200kN. Due to the symmetry of the pipe, the boundary condition and the applied loads, only a quarter of the pipe was used in the analysis as shown in Figure 9.2. The boundary conditions in the analysis included the nodes fixed at the pipe bottom, and the symmetrical conditions on the plane $x = 0$ and $y = 0$.

In the back analysis, the concrete pipe was assumed to have the same elastic material constants as the model pipes used by Ripley (1989), the Young's modulus E_c = 31700MPa and the Poisson's ratio μ_c = 0.22, since they were constructed with the ingredients in the same ratio (refer to Table 8.1 in Chapter 8). To model the stress redistribution in the pipe without using complex concrete models, a modified Matsuoka model described in Chapter 2 was used for the concrete pipe in the back analysis. From the characteristic tests described in Chapter 8, it is known that the cube strength and the compression strength of the concrete pipe in the experiment were about 60MPa and 50MPa respectively. When a typical ratio of $\frac{1}{10}$ (Jiang and Feng 1991, Neville 1981) between the tensile and compression concrete strength was used with an associated flow rule, the material parameters with this model in the analysis were a triaxial frictional angle $\phi = 54.9^0$, a triaxial dilation angle $\psi = 54.9^0$ and a tensile strength f_t = 5MPa.

As discussed in Chapter 2, the modified Matsuoka model does not consider the cracking behaviour of the concrete which is beyond the scope of the current project, instead the maximum tensile stress in the concrete pipe was restricted to be below or equal to the tensile strength of the concrete in this model. This means that the back analysis described in this Chapter didn't examine the cracking behaviour of the concrete pipe and the failure load. Rather, the aim was to understand the working mechanism of the local reinforcement and the local prestressing and to confirm the experimental results.

9.2 BACK ANALYSIS OF LOCAL REINFORCEMENT

The extended back analysis of the local reinforcement is described in this section. In order to include the effect of the location of the reinforcement, the back analyses were extended with three different cases, the case CR with the plane pipe (without reinforcements), the case RE1 with the reinforcements near to the external pipe surface as used in the

experimental tests and the case RE2 with the reinforcements near to the internal surface of the pipe. In the analysis, 8-node brick elements and 3-node bar elements were used. The finite element meshes are shown in Figure 9.2(a), 9.2(b) and 9.2(c) for the CR, RE1 and RE2 respectively. The quarter of the pipe used in the analysis was between $\theta = 90^0$ and $\theta = 180^0$ as shown in Figure 9.2(d). The reinforcements were modelled by elastic bar elements (refer to Section 2.5 in Chapter 2). A typical steel Young's modulus E_{st} = 200GPa was used for the steel bars and the cross sectional area of the bar was $A = 6.28mm^2$ as shown in Figure 8.7 in Chapter 8. For simplicity, the bond between the reinforcing bars and the concrete was considered to be perfect. The analysis was carried out using the modified Newton-Raphson method described in Chapter 2. The number of calculation steps was 400.

To examine the pipe performance, only the stresses in the concrete pipe are discussed and presented in this chapter with the stresses in the reinforcing steel bars excluded. The most tensile principal stresses within the concrete pipe are shown in Figures 9.3(a), 9.3(b) and 9.3(c) for the cases CR, RE1 and RE2 respectively. From the figure, it is clearly seen that the tensile stresses in all three cases have similar distribution patterns and reach the tensile strength (5MPa) in the region of $\theta = 90^0$ on the internal surface at first (the tensile stresses are mainly in the hoop direction). This possibly explains why there are many cracks found on the internal surface of the pipe after failure. However, the size of the domain with high tensile stresses in the cases of RE1 and RE2 is smaller than that in the case of CR because the reinforcing bars have undertaken some of the tensile stresses, especially in the case of RE2.

The most tensile principal stresses within the pipe viewed from the opposite direction are shown in Figures 9.4(a), 9.4(b) and 9.4(c) for the cases CR, RE1 and RE2 respectively (the region of $\theta = 180^0$ is at the right side in Figure 9.4). Again, the figure shows that the stress distribution patterns are similar to some extent in all three cases and the high tensile stresses are mainly located at or near the pipe joint, where the pipe usually failed during the laboratory tests. Moreover, the results indicate that with the reinforcements at the pipe joint, cracks may

first appear in the region of $\theta=180^0$ below the reinforcement on the external surface as found during the tests (refer to Section 8.7 in Chapter 8). The maximum tensile stress reduces in the cases of RE1 and RE2 compared with that in the case of CR due to the effect of the reinforcing steel bars.

From the discussion above, the back analysis clearly shows that the tensile stresses first reach the tensile strength on the internal surface in the region $\theta = 90^0$ at the right top corner of the pipe, then the tensile stresses redistribute into the adjacent region and across the pipe thickness towards the external surface of the pipe due to the failure of the concrete (in the current material model, this means the concrete cannot take more tensile stresses); and that the reinforcements take some tensile stresses over from the failed concrete and improve the pipe's performance. Moreover, the reinforcements in the case RE2 have a greater effect than those in the case RE1 because the high tensile stresses are mainly located on the internal surface of the pipe. In practice, due to the cracking (which is not considered in the current project), the concrete would soon lose its capacity to sustain tensile stresses after reaching the tensile strength (Jiang and Feng 1991, Neville 1981), and the stress redistribution would be quicker and larger than that predicted in this back analysis. This means the effect of the reinforcements could be bigger than that shown in Figures 9.3 and 9.4 especially in the case of RE1. In order to examine the detailed failure mechanism in the reinforced concrete pipe, a complex material model is needed.

9.3 BACK ANALYSIS OF LOCAL PRESTRESSING

The extended back analysis of the local prestressing is described in this section. The prestressing was applied at the pipe joint by a steel band as shown in Figure 9.5(a) before the pipe was fixed on the bottom steel block (refer to Section 8.6 in Chapter 8). To model this problem, there were two analysis stages in the back analysis. At first, a uniform pressure

from the prestressed steel band was applied on the external surface of the plain concrete pipe at the joint with the pipe simply supported at the bottom as shown in Figure 9.5(c); the finite element mesh was the same as shown in Figure 9.2(a) for the plain pipe; and the boundary conditions included the nodes pinned at the pipe bottom and the symmetrical conditions on the plane of $x = 0$ and $y = 0$. In the second analysis stage, for simplicity the prestressed steel band was modelled as elastic reinforcing bars at the external surface of the pipe as shown in Figure 9.5(b), and the applied load and boundary conditions were the same as those described in Section 9.2. The cross sectional area of the steel band was $A = 18mm^2$ as shown in Figure 9.5(a) (the middle reinforcing bar had a cross sectional area of $9mm^2$ and the cross sectional area for the other two bars was $4.5mm^2$). The bond between the reinforcing bars and the concrete was again treated as perfect and the steel Young's modulus was $E_{st} = 200GPa$. Only a quarter of the pipe was used in the analysis due to the symmetry of the pipe, the loading condition and the constraint conditions. To examine the influence of the magnitude of the local prestressing, the back analyses were also extended with two cases, the case PR1 with $q = 5MPa$ which was calculated from the experimental data and the case PR2 with $q = 1MPa$. Again, the analysis was carried out using the modified Newton-Raphson method. The number of calculation steps was 50 for the first analysis stage and 400 for the second stage.

The most tensile principal stresses within the concrete pipe (the stresses in the steel band are not included) are shown in Figures 9.6(a) and 9.6(b) for the case of PR1 and PR2 respectively, while Figures 9.6(c) and 9.6(d) show the most tensile principal stresses viewed from the opposite direction (that is, the region of $\theta = 180^0$ is at the right side in Figures 9.6(c) and 9.6(d)). Comparing with the stresses in Figure 9.3(a) in Section 9.2, it is clear that the stress distribution patterns on the internal surface are somewhat similar in the cases of CR, PR1 and PR2. However, the high stress domains in the case of PR1 and PR2 are smaller than that in the case of CR, especially in the case of PR1. On the external surface of the pipe, the high stresses are located below the steel band which is the region in which cracks

were first spotted during the tests. The maximum tensile stress in the case of PR2 is lower that that in the case of CR, however, in the case of PR1, the maximum tensile stress is higher.

From the discussion above, it is clear that the local prestressing is very effective to reduce the tensile stresses on the internal surface of the pipe at the pipe joint due to the compressive stresses produced by the prestresses on the external pipe surface (Timoshenko and Goodier 1970). Furthermore, the steel band also reduces the tensile stresses on the external surface of the pipe acting as reinforced steel bars. However, the magnitude of the prestress should be controlled well to avoid a worse situation on the external surface of the pipe due to the local effect. The results in the back analysis also show that the magnitude of the prestresses used in the experiment in Chapter 8 are slightly higher than necessary because it worsens the tensile stresses on the external surface of the pipe. This is possibly the reason why the local reinforcement gives a better improvement in the pipe performance than the local prestressing in the experiment.

9.4 DISCUSSION

From the discussion above, the back analysis described in this chapter demonstrates the improvement of the stresses in the concrete pipe with the local reinforcement and the local prestressing using a simple modified Matsuoka model. In general, the location of early cracks spotted during the test agree well with the region of high tensile stress in the analysis. The results in this chapter confirm the improvement of the use of local reinforcement and local prestressing. This means that the local reinforcement and the local prestressing can be applied to improve the design of prototype concrete pipe. Due to the complicated nature of the problem, the final failure mechanism and the failure load are out of the scope of this back analysis. Further research is needed to examine the cracking behaviour of the concrete in order to have a better understanding of the pipe's performance in practice.

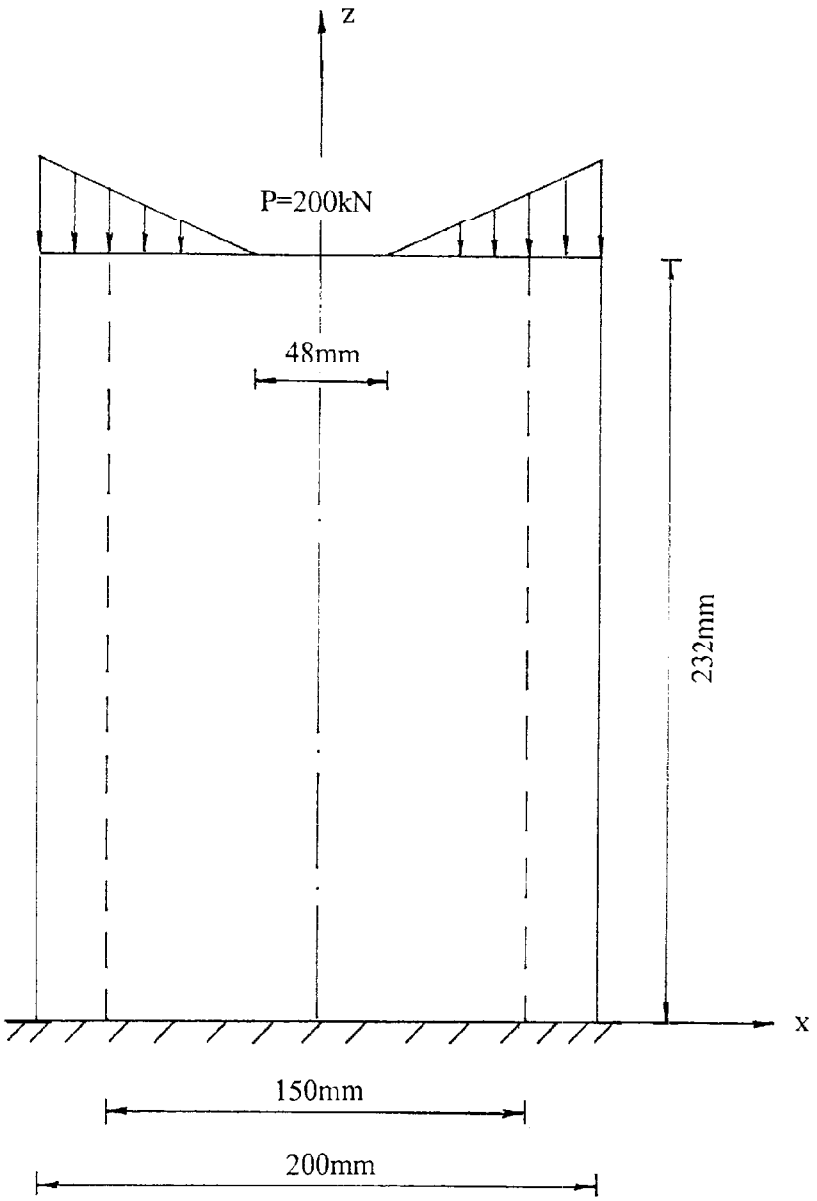


Figure 9.1 Loading and boundary condition of the tests

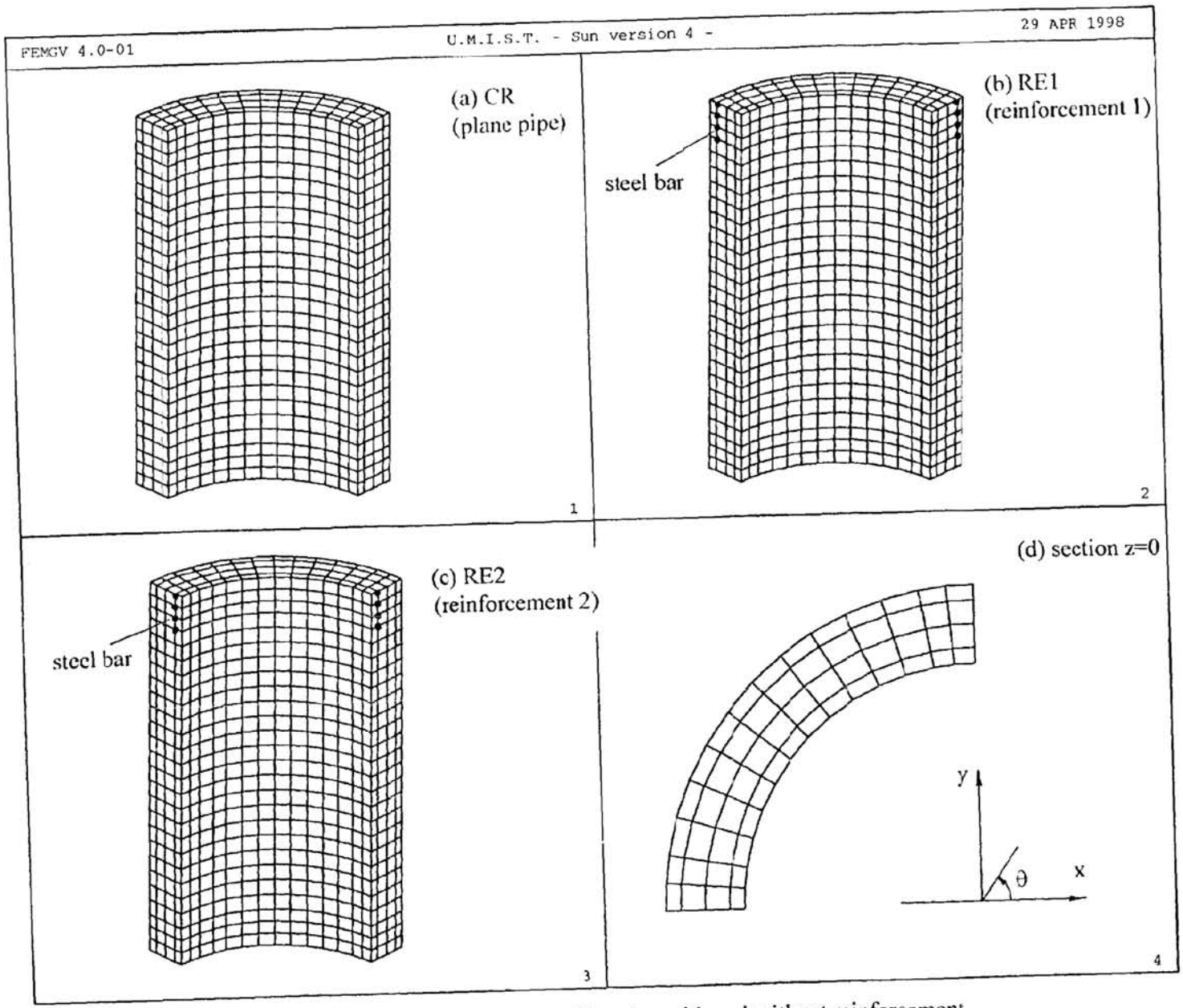


Figure 9.2 Finite element meshes of the pipe with and without reinforcement

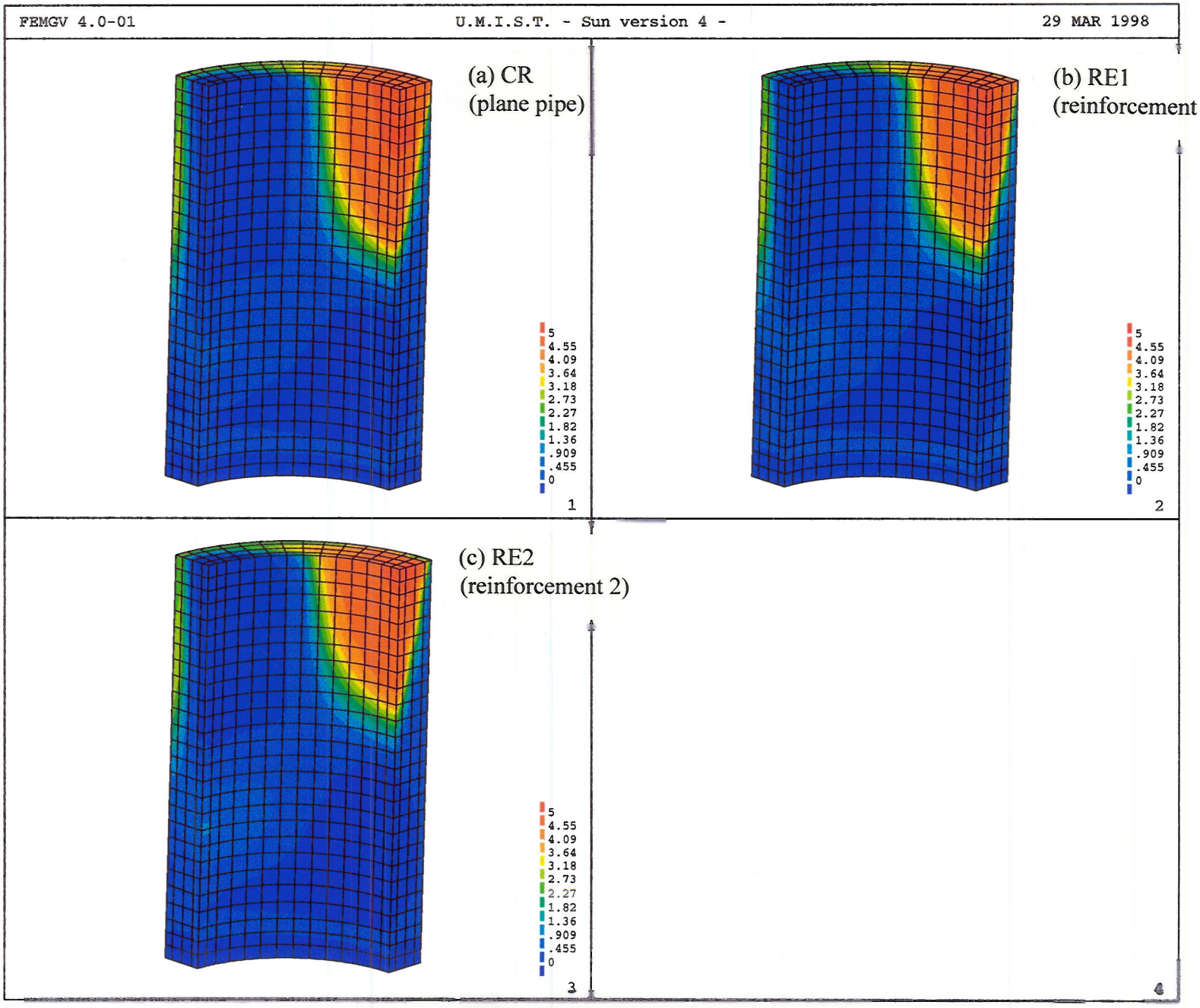


Figure 9.3 Most tensile principal stresses in the concrete pipe with and without reinforcement (MPa)

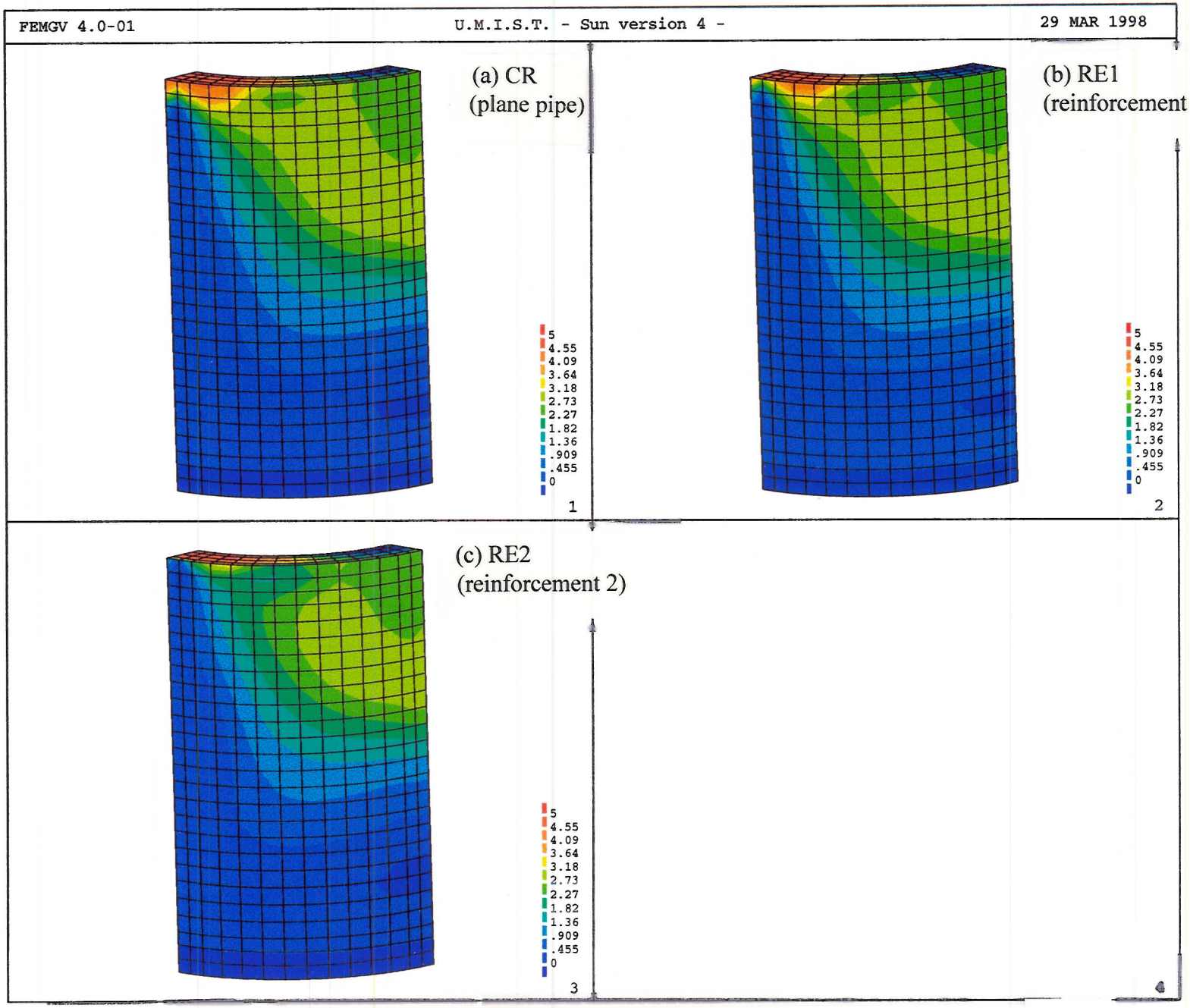


Figure 9.4 Most tensile principal stresses in the pipe viewed from the opposite direction (MPa)

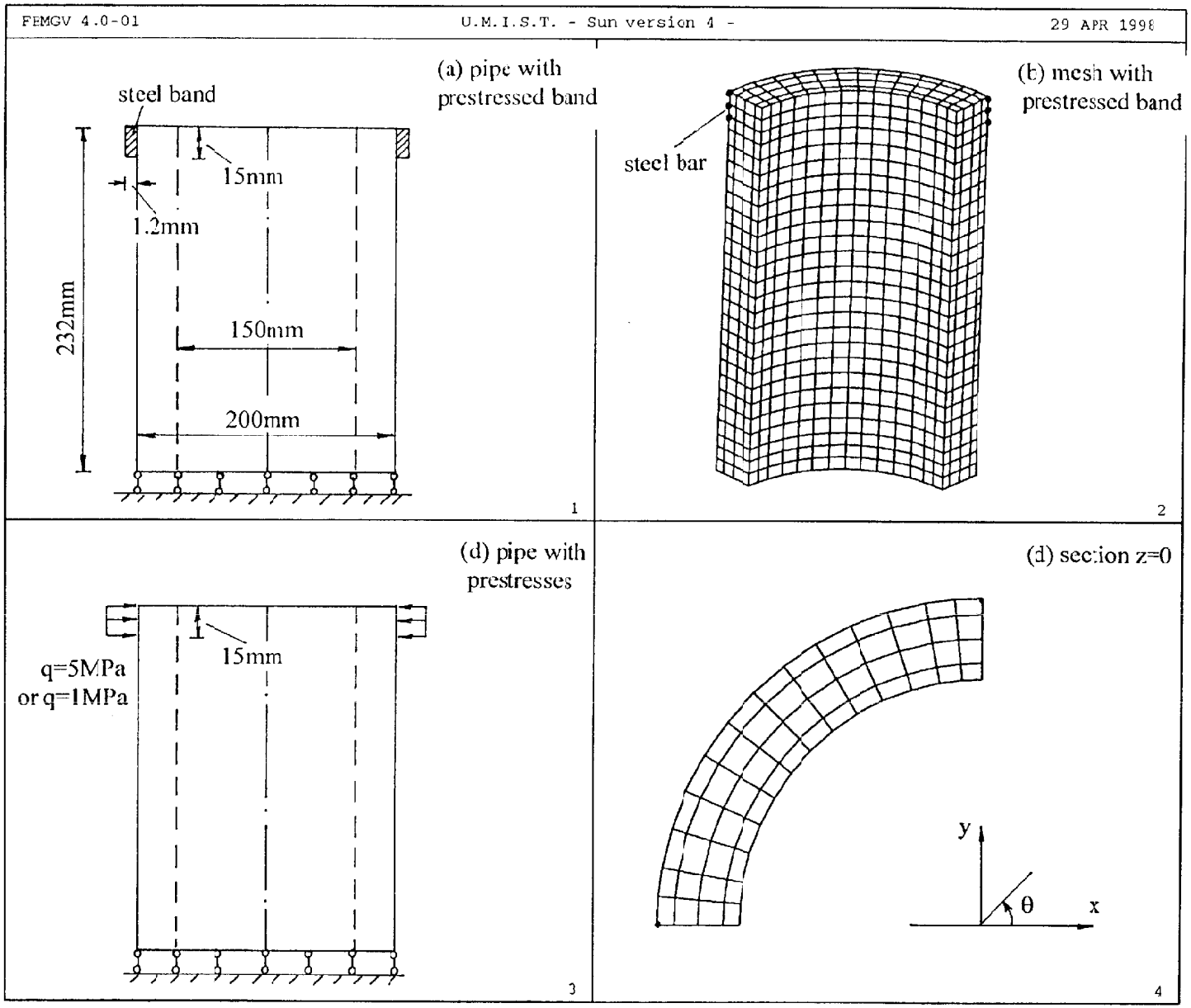


Figure 9.5 Local prestressing and the corresponding finite element mesh

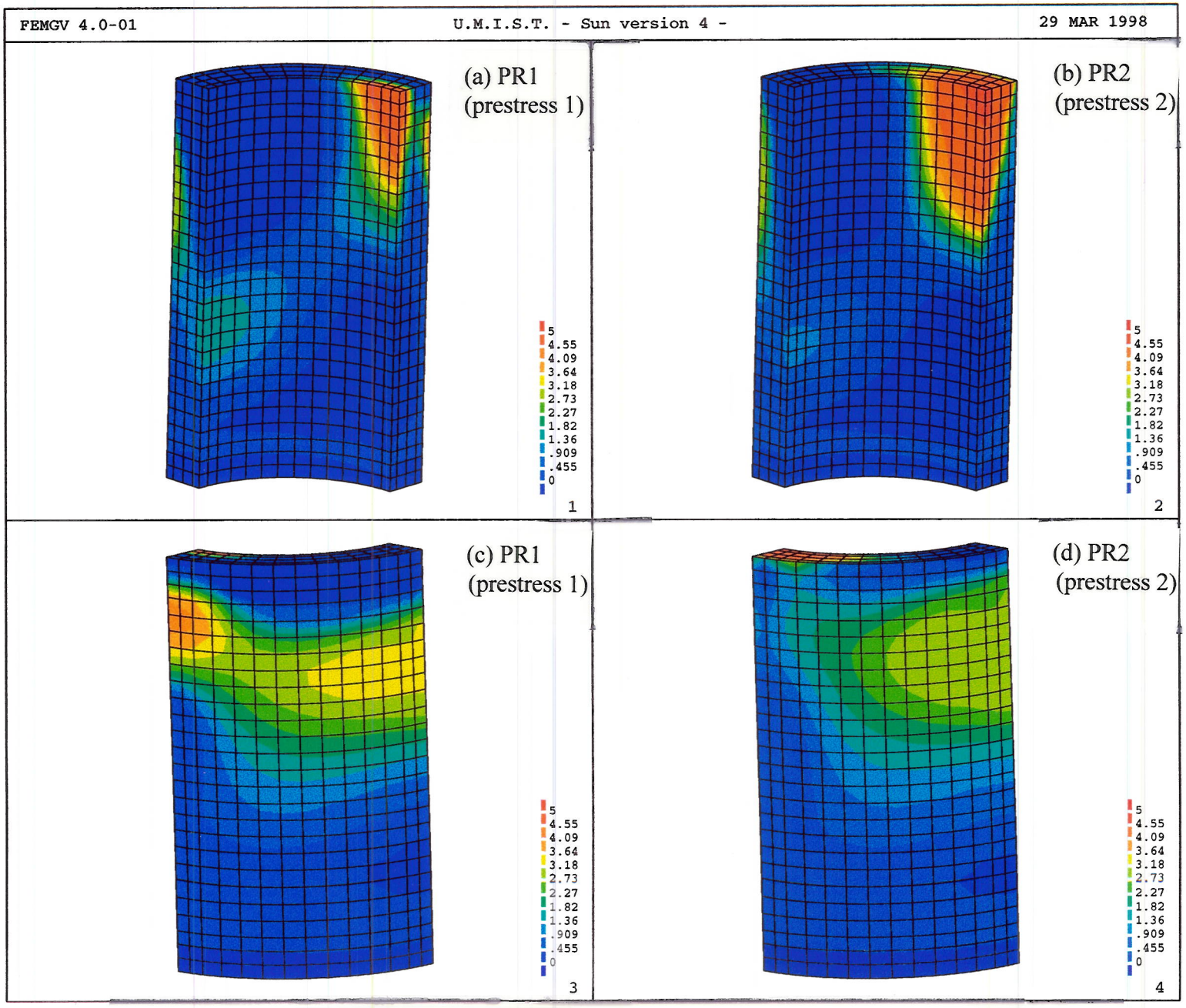


Figure 9.6 Most tensile principal stresses in the concrete pipe with prestressing (MPa)